mater.scichina.com link.springer.com

Published online 22 February 2024 | https://doi.org/10.1007/s40843-023-2759-9
Sci China Mater 2024, 67(3): 974–982

Accelerating structural relaxation of shear band at ambient conditions through cryogenic thermal-cycling

Yufeng Wei[1], Jie Pan[1,2*], Yonghao Sun[3,4*], Ning Li[1], Cheng Zhang[1], Weihua Wang[3,4] and Lin Liu[1*]

ABSTRACT **Cryogenic thermal-cycling (CTC) is a promising method for the rejuvenation of metallic glasses (MGs). Although seemingly arbitrary, the direction of energy change in MGs following CTC sometimes results in relaxation rather than rejuvenation. By demonstrating enthalpy relaxation in a shear band (SB) and enthalpy rejuvenation in the metallic-glass matrix, the current work demonstrates that the initial state of the specimen matters. Micro-hardness, nano-indentation loading curves, and the shapes of indents all support the bidirectional trends. Notably, after subjecting the specimen to 100 cryogenic thermal-cycles, the enthalpy and hardness tend to converge into an equilibrium value. It is discovered that CTC can accelerate the structural relaxation of SB at room temperature, a phenomenon that thermal annealing at the upper temperature (353 K) of CTC cannot achieve. Additionally, the experimental results have been elucidated by adapting the free-volume model. The work provides new insights into the functionalities of CTC and illuminates the initial state of the metallic-glass sample upon reversing the direction of enthalpy change.**

Keywords: metallic glasses, cryogenic thermal-cycling, rejuvenation, relaxation, energy state

INTRODUCTION

Since its first publication in 2015, the cryogenic thermal-cycling (CTC) technique has received great attention in the field of metallic glasses (MGs). Simply by submerging the MG ribbons or rods in liquid nitrogen, then removing them to ambient conditions, and repeating the process for several tens or hundreds of rounds, structural rejuvenation has been discovered in various MG compositions [1–4]. Rejuvenation drives MGs towards higher enthalpy levels, increased structural disordering, as well as improvements in mechanical performances such as plasticity [1,5–8] and fracture toughness [9,10], in contrast to structural relaxation that is associated with energy reduction, structural ordering, and deterioration of mechanical properties [11,12]. The CTC technology stands out among other alternatives [13–15] for rejuvenating MGs because of its ease of use, low cost, and non-destructive nature [16]. Many efforts have been made in recent years to increase the number of thermal cycles (TCs) to approximately a thousand [17] or to investigate stress-cycling at ultrasonic frequencies [18].

New questions start arising as a result of more studies published on this subject. While many MG compositions exhibit rejuvenation after CTC, examples like $Ti_{41}Zr_{25}Be_{29}Al_5$ [19] and $Fe_{80}P_{20}$ [20] MGs display relaxation instead. According to Ketkaew *et al.* [10], depending on the chemistry of the alloying components and the fictive temperature of the glassy structure, the conditional fracture toughness of as-cast MGs behaves differently upon CTC, showing either rejuvenation or relaxation. Intriguingly, partially-relaxed samples exhibit the strongest rejuvenation performance, suggesting that the CTC effects may be influenced by the initial state of the MG sample [21]. Furthermore, it has been suggested that the CTC effects could disappear after one week due to the anelastic recovery [4]. For these somewhat contentious observations to be explained, new theories and tests are urgently needed.

An analogy can be drawn between the energy storage mechanisms of MGs through thermo-mechanical processing (TMP) and CTC. The core concept of the TMP theory [22] revolves around the equilibrium state, represented by either enthalpy or free volume. The equilibrium state is influenced by temperature and strain rate, which essentially represents a competition between creating free volume (or increasing enthalpy) and annihilating free volume (or decreasing enthalpy). Rejuvenation happens when the equilibrium state has an energy higher than the starting state; on the other hand, relaxation happens when the equilibrium state has an energy lower than the starting state. However, to the best of our knowledge, no one has ever systematically examined the validity of TMP theory for CTC using MG samples starting from varied initial states. The structural and physical variations of the MG specimens may be a challenge. The same sample should be used for the CTC treatment in order to improve reproducibility.

In this work, a composite structure with a single shear band (SB) in the MG matrix was designed [23]. The SB undergoes substantial plastic deformation, resulting in extensive rejuvenation and a remarkable maximum energy storage capacity of 45 J g^{-1} when the SB width in relation to its specimen thickness is taken into account [23]. In comparison to the SB, the matrix is

[1] School of Materials Science and Engineering, State Key Lab for Materials Processing and Die & Mold Technology, Huazhong University of Science and Technology, Wuhan 430074, China
[2] Shenyang National Laboratory for Materials Science, Institute of Metal Research, Chinese Academy of Sciences, Shenyang 110016, China
[3] Institute of Physics, Chinese Academy of Sciences, Beijing 100190, China
[4] Songshan Lake Materials Laboratory, Dongguan 523808, China
* Corresponding authors (emails: jpan@hust.edu.cn (Pan J); ysun58@iphy.ac.cn (Sun Y); lliu2000@mail.hust.edu.cn (Liu L))

relatively relaxed, i.e., the matrix has an energy lower than that of the SB. To investigate how the initially-rejuvenated SB and initially-relaxed matrix (both contained in one specimen) respond, such MG composites are treated in CTC. The findings show that CTC behaves as predicted by the TMP theory and, intriguingly, that CTC can speed up structural relaxation at temperatures too low for thermal annealing.

METHODS

Bulk MGs with a nominal composition of $Zr_{69.5}Cu_{12}Ni_{11.5}Al_{7.5}$ (in atomic % hereafter) were fabricated by arc-melting the constituent elements in a Ti-gettered, high-purity argon atmosphere. Suction casting was used to produce cylindrical rods with a 2 mm diameter after the master alloy, which was remelted six times to ensure chemical homogeneity. X-ray diffraction (XRD, Shimadzu 7000SX) with Cu-Kα radiation and a high-resolution transmission electron microscope (HRTEM, FEI Tecnai F20) were used to confirm the amorphicity of the specimens before and after the CTC (Fig. 1). Differential scanning calorimetry (DSC, TA Q2000) was employed to measure the thermal response of the specimens at a heating rate of 20 K min^{-1}. The first run was stopped at 800 K, the temperature at which crystallization ends, and the second run was monitored under identical conditions to serve as a baseline. The glass transition temperature T_g is 620 K. The error of the enthalpy measurement is about 0.3 J g^{-1}. The cast rods were cut into specimens for compression tests with a diameter of 2 mm and a length of 4 mm, and the ends were carefully polished to guarantee parallelism. It was ensured that the direction of force loading was consistent with the central axis of the sample during the compression process. The compression test was performed using a Zwick/Roell 020 compression tester with a strain rate of 2×10^{-4} s^{-1}. A diamond pyramid indenter was used to conduct the Vickers hardness test, with a weight of 50 g and a dwell time of 10 s. Under loading-rate control (0.5 mN s^{-1}), nano-indentation was carried out utilizing an Agilent Nano Indenter G200 and a diamond Berkovich indenter. Atomic force microscopy (AFM, Shimadzu SPM9700) was applied to examine the indent morphology. Each experiment was conducted at least three times, with the averaged results being recorded.

By carefully regulating the strain rate of deformation, MG samples with a single SB were produced. After the total strain reached 8.5%, compression was manually stopped (Fig. 2a). The shear step, as indicated in Fig. 2b, was between 30 and 40 μm. For DSC tests, the regions marking the matrix (without SBs) were sectioned from the sample bottom, while the regions containing SBs were sectioned from the sides of the SBs (as shown in Fig. 2b). As the distribution of enthalpy around the SB is non-uniform after deformation, the measured enthalpy values are influenced by the thickness of sample containing SB [23]. To maintain a constant thickness of the sample containing SB for calorimetry testing, the specimens before and after CTC were sectioned to a thickness of about 200 μm. For indentation tests, the whole specimens were sectioned vertically, carefully polished, and then subjected to indentation testing. The SB was indented along a line at a 30° angle, and the distance between adjacent indents was 20 μm for microhardness testing (twice the size of the indents) and 10 μm for nano-indentation testing (ten times the size of the indents). Following the CTC treatment, further indentations were made on the same specimen along lines parallel to the first with a spacing of 50 μm. The samples were subjected to CTC treatments by being submerged in liquid nitrogen (at 77 K) for 1 min, removed, and then inserted into a furnace that was kept at 353 K (Fig. 2c). The samples were put through one TC by being submerged again in liquid nitrogen. TCs ranging from 10 to 100 times were used in our tests.

THEORY

We begin by modeling free-volume creation. The defects in MGs are often described by the free volume model [24], in which they are density fluctuations with volume greater than a critical value v^*. The defect concentration c_f is described by

$$c_f = \exp\left(-\frac{\gamma v^*}{v_f}\right) = \exp\left(-\frac{1}{x}\right), \quad (1)$$

where γ is a geometrical factor taking 0.8, and v_f is the average free volume per atom. The quantity $x = v_f/\gamma v^*$ is the reduced free-volume.

The creation of defects during plastic deformation is induced by shear, and the rate of which can be described as [25]

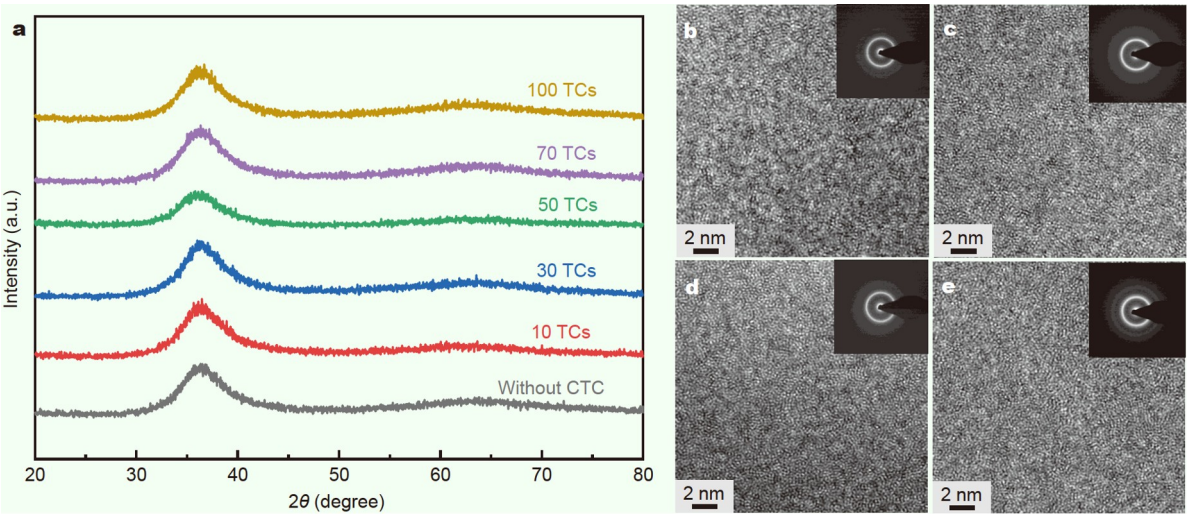

Figure 1 Structural characterization of the as-cast and the CTC-treated $Zr_{69.5}Cu_{12}Ni_{11.5}Al_{7.5}$ MG samples. (a) XRD patterns. HRTEM images of various parts of the metallic-glass sample: (b) matrix without CTC; (c) SB without CTC; (d) matrix after 50 TCs; (e) SB after 50 TCs.

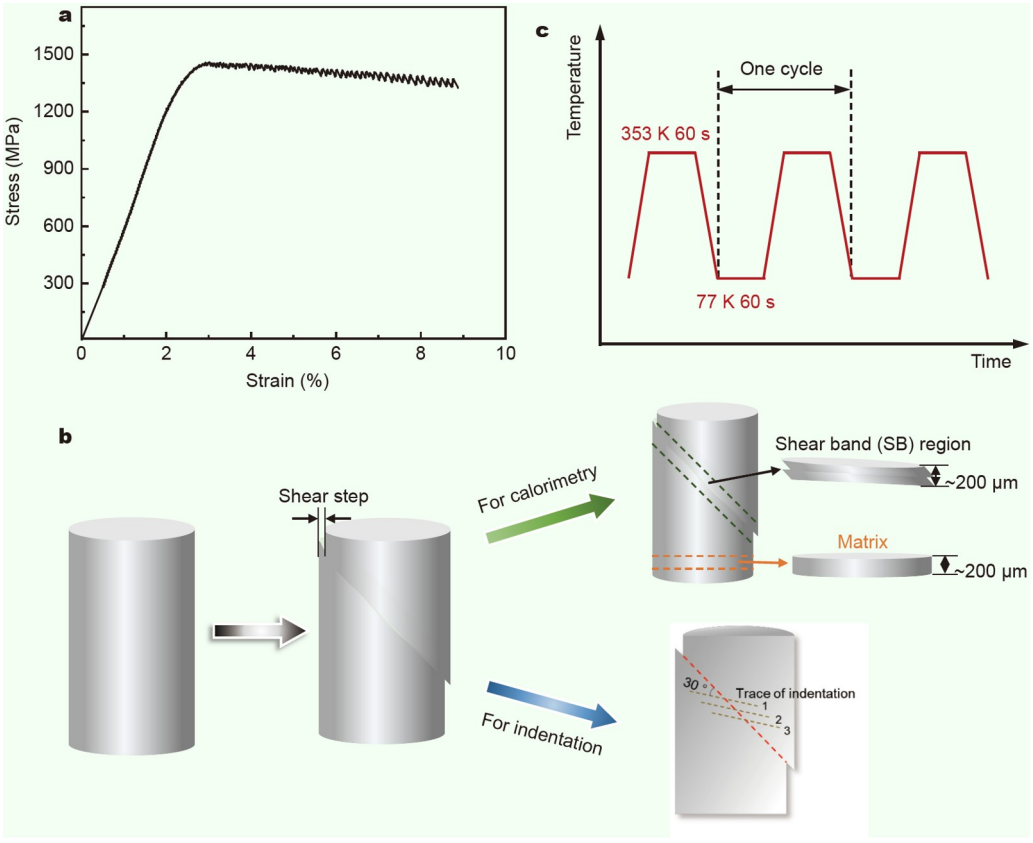

Figure 2 (a) Engineering stress-curve of $Zr_{69.5}Cu_{12}Ni_{11}Al_{7.5}$ MG; (b) the SB and the matrix parts applied for DSC tests; (c) the thermal protocol of CTC, and the schematic diagrams specifying.

$$\frac{dv_f}{dt} = 2c_f kT\frac{3(1-\vartheta)\gamma v^*}{2\mu(1+\vartheta)v_f}f\exp\left(-\frac{\Delta G^m}{kT}\right)\left[\cosh\left(\frac{\tau\Omega}{2kT}\right)-1\right], \quad (2)$$

where k is the Boltzmann constant with a value of 1.38×10^{-23} J K^{-1}, T is the temperature, ϑ is the Poisson's ratio, μ is the shear modulus, f is an attempt frequency, ΔG^m is the activation energy, τ is the shear stress, and Ω is the activation volume that is close to the atomic volume. Thus, the free-volume generation rate is [26]

$$\Delta^+\dot{x} = \frac{2fkT}{x\gamma Sv^*}\exp\left(-\frac{\Delta G^m}{kT}\right)\exp\left(-\frac{1}{x}\right)\left[\cosh\left(\frac{\tau\Omega}{2kT}\right)-1\right]. \quad (3)$$

We now turn to modelling free-volume annihilation. The annihilation of free volume takes place by a bimolecular process, and the rate of free-volume annihilation can be described as [25,27]

$$\left.\frac{dc_f}{dt}\right|^- = -f\exp\left(-\frac{\Delta G_m}{kT}\right)c_f(c_f-c_{f,eq}), \quad (4)$$

where $c_{f,eq}$ is the free-volume concentration of the metastable equilibrium supercooled liquid. For CTC, there are two unique aspects. The first aspect is $c_{f,eq}$ that is given by a Fulcher-Vogel type equation as

$$c_{f,eq} = \exp\left(-\frac{B}{T-T_0}\right), \quad (5)$$

where B and T_0 are the fitting constants ($T > T_0$). Cohen and Turnbull [24] defined T_0 as the ideal glass-transition temperature, which should be approximately $0.85T_g$ for glasses [28]. Since the cryogenic temperatures applied to our Zr-based MG are far below its T_0, $c_{f,eq}$ can be considered as zero. Therefore, Equation (4) can be simplified as [25]

$$\left.\frac{dc_f}{dt}\right|^- = -f\exp\left(-\frac{\Delta G_m}{kT}\right)c_f{}^2. \quad (6)$$

The second aspect is ΔG_m. Jin *et al.* [29] introduced a $P\Delta V_m$ term to ΔG_m, making it harder to cross the energy barrier for free-volume annihilation under pressure (P), where the volumetric change ΔV_m is about 0.8Ω. Wang *et al.* [26] introduced a $-\sigma_m\Delta V_m$ term to ΔG_m in order to lower the energy barrier for free-volume annihilation under tensile pressure (σ_m). Considering that neither compressive nor tensile pressure would be expected in CTC, we proposed that τ, which is generated by the internal deformation of heterogeneities under CTC, leads to densification or free-volume annihilation at large values of x. Shear is thought to cause dilation but we argued that it only works at small values of x. Actually, Pan *et al.* [5] demonstrated strain-hardening of a highly-rejuvenated MG whose initial x must be big, lending credence to this. They specifically showed that the reciprocal vector of the first diffraction peak q_1 of the rejuvenated sample increases with plastic strain. Because Ω is the atomic volume and $q_1\cdot\Omega^{0.433} = 9.3$ [30], a rise in q_1 denotes a fall in Ω or densification. In contrast, they also demonstrated that shear-induced dilatation is likely the cause of q_1 decreasing with plastic strain for as-cast starting from a small value of x. Therefore, using Equations (1 and 6), together with the addition of $-\tau\Delta V_m$ to ΔG_m (also valid for Equation (3)), the free-volume

annihilation rate is

$$\Delta^{-}\dot{x} = -fx^{2}\exp\left(-\frac{\Delta G^{m}-\tau\Delta V_{m}}{kT}\right)\exp\left(-\frac{1}{x}\right). \quad (7)$$

Combining Equations (3 and 7), finally, the free-volume rate $\Delta\dot{x}$ is

$$\Delta\dot{x} = \frac{2fkT}{x\gamma Sv^{*}}\exp\left(-\frac{\Delta G^{m}-\Delta V_{m}}{kT}\right)\exp\left(-\frac{1}{x}\right)\left[\cosh\left(\frac{\tau\Omega}{2kT}\right)-1\right] - fx^{2}\exp\left(-\frac{\Delta G^{m}-\Delta V_{m}}{kT}\right)\exp\left(-\frac{1}{x}\right), \quad (8)$$

and the reduced free-volume is

$$x = x_{0} + \int_{0}^{t}\Delta\dot{x}\mathrm{d}t, \quad (9)$$

where t is time or deformation period, and x_0 is the initial x in the tested MG. This work follows Ref. [26] using exactly the same fitting parameters of T = 300 K, γ = 0.15, f = 5.415×10^{12} s^{-1}, Ω = 2.424×10^{-29} m^3, μ = 28.5 GPa, v^{*} = 1.939×10^{-29} m^3, ΔG^{m} = 1×10^{-19} J, and ν = 0.377. By illustrating how x_0 affected the changing direction of x, we were able to study how the initial state of MG influenced rejuvenation and relaxation.

RESULTS

Calorimetry

By incorporating an SB into an MG rod before CTC treatments, it is possible to assess the CTC response of a single specimen with a composite structure made up of both rejuvenated and relaxed regions in a high-throughput way. The idea is supported by the DSC results. As seen in Fig. 3, the enclosed region between the first and second heating runs of the SB section (without CTC) is noticeably bigger than that of the matrix (without CTC). The heat of relaxation (ΔH_{rel}), as indicated by the area of the enclosed region of the SB section, is twice that of the matrix (10.7 J g^{-1}/5.5 J g^{-1} ≈ 2). These results support the hypothesis that the SB is in a rejuvenated state, whereas the matrix is in a relatively relaxed state. Although compositional deviation in the SB is under debate, we argue that the deviation should be disregarded because the scale of phase separation (within 10 nm of the SB width) is much smaller than the dimensions of the materials employed for DSC testing (200 μm in thickness) and indentation (all indents are concentrated in a line of 300 μm in length) tests. This viewpoint is consistent with the synchrotron XRD observation, which claims that despite of a 3% density reduction in SB, its average chemistry is unchanged [31]. Therefore, the compressed specimen emerges as a promising candidate for comprehending how CTC treatment affects the MGs with various initial energy-states.

After being treated by 100 TCs, the SB and matrix sections of the compressed rods were cut for DSC tests. An increase in ΔH_{rel} signifies rejuvenation, while a decrease in ΔH_{rel} represents relaxation. As seen in Fig. 3, the ΔH_{rel} value of the matrix section after 100 TCs is 6.3 J g^{-1}, which is 14.5% higher than the matrix without CTC (5.5 J g^{-1}). The ΔH_{rel} value of the SB section after 100 TCs is 7.1 J g^{-1}, which is 33.6% less than that of the SB without CTC (10.7 J g^{-1}). These results confirm the bidirectional action of CTC on MG. CTC causes rejuvenation when the starting state is at lower energy (for example, the matrix), while it causes relaxation when the initial state is rejuvenated (for instance, the SB). These findings might help to understand why the CTC rejuvenates some MGs while relaxes others [10]. Given that the 6.3 J g^{-1} of the matrix is not far from the 7.1 J g^{-1} of the SB, it appears that the ΔH_{rel} of the matrix and SB tend to converge towards a similar value after undergoing 100 TCs. This observation suggests that the equilibrium value of ΔH_{rel}, which might be attained in additional TCs. Besides, it is noteworthy that during CTC, the matrix absorbs energy from the environment rather than the SB. According to Fig. 2, the volume of the SB section ($0.2\pi\times\sqrt{2}$ = 0.889 mm^3) only occupies 7% of the sample volume ($0.25\pi\times2^2\times4$ = 12.56 mm^3). Since the SB

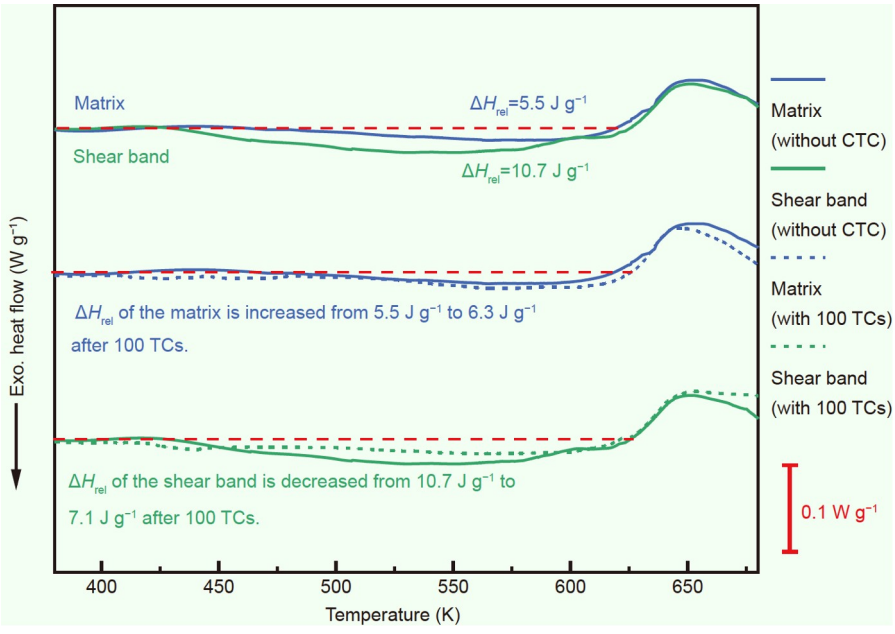

Figure 3 DSC heating curves the SB (green) and the matrix (blue) parts before (solid) and after (dashed) 100 TCs. Correspondingly, the heat of relaxation (ΔH_{rel}) is calculated from the area enclosed by the heating curves of MG parts and the baseline of the crystallized (red-dashed line).

section reduces its ΔH_{rel} by 3.6 J g^{-1}, the energy that the SB can provide is 0.3 J g^{-1} (3.6 × 7% ≈ 0.3 J g^{-1}) at most. Even if the matrix completely absorbs all the heat released by the SB, there would still remain an excess of 0.5 J g^{-1} (6.3 − 5.5 − 0.3 = 0.5 J g^{-1}), which is two-thirds of the total heat absorption.

Micro-indentation

Micro-hardness tests were conducted on the vertically sectioned sample (Fig. 2b). Thirty indents were made, following a line trace and crossing the SB. Within a width of roughly 160 μm, significant softening and a V-shaped pattern in the micro-hardness (H_V) values is seen surrounding the SB (Fig. 4). The matrix has an averaged H_V of 400 kg mm^{-2}, while the SB has an averaged H_V of 314 kg mm^{-2} near its center. The initial states of the matrix and the SB center are represented by their H_V difference of 86 kg mm^{-2}.

The gap between the matrix and the SB center begins to narrow upon CTC. After 30 TCs, the H_V of the SB center increases to 332 kg mm^{-2}, while the averaged H_V of the matrix decreases to 385 kg mm^{-2}, leaving a gap of 53 kg mm^{-2}. After 50 TCs, the increase in H_V of the SB center is obvious since it adds up to 343 kg mm^{-2}, but the change in H_V of the matrix is less noticeable, leaving a gap of roughly 42 kg mm^{-2}. After 100 TCs, the H_V at the SB center ramps to 362 kg mm^{-2}, while that of the matrix decreases to 376 kg mm^{-2}, narrowing the gap to 14 kg mm^{-2}. Additionally, the width of the softening zone is decreased. The width begins at 160 μm, shrinks to 90 μm (after 30 TCs), and finally ends at 10 μm (after 100 TCs). Although the central part of the SB has a hardness still lower than the matrix, the difference is within the margin of measurement error. Consequently, at least three factors are included in the effects of CTC: (1) the rejuvenated becoming harder; (2) the relaxed becoming softer; and (3) the rejuvenated and the relaxed reaching the same H_V.

To assess the stability of SB relaxation caused by CTC, we remeasured the H_V of the CTC-treated sample (200 TCs) after one year. It is possible that the CTC has permanently altered the structure of SB because there is no decline in the elevated *Hv* of the SB (Fig. 5a). For comparison, we also subjected the SB sample (without CTC) to annealing at room temperature for one year. The *Hv* of the SB continues to exhibit the V-shaped distribution, with only a slight increase in the values (Fig. 5b), proving that the SB remains relatively stable at room temperature. Consequently, it can be inferred that the rejuvenation caused by SBing is not a transient effect. The CTC process indeed causes permanent structural relaxation of SB.

Nano-indentation

Nano-indentation tests were conducted on another compressed specimen. Fig. 6a presents the load (*F*) *vs.* depth (*h*) curves

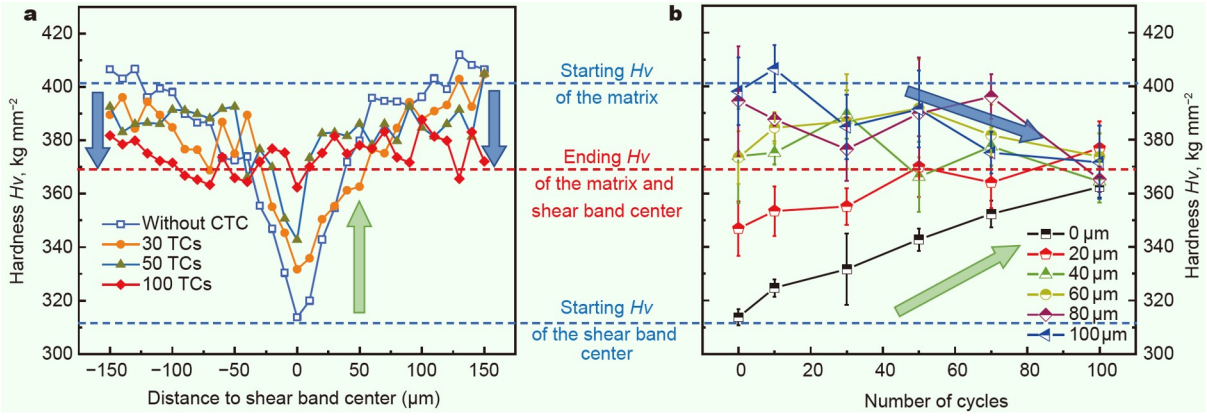

Figure 4 (a) Microhardness (H_V) profile across the SB of the samples subjected to varying numbers of cycles; (b) microhardness evolution of different regions under CTC.

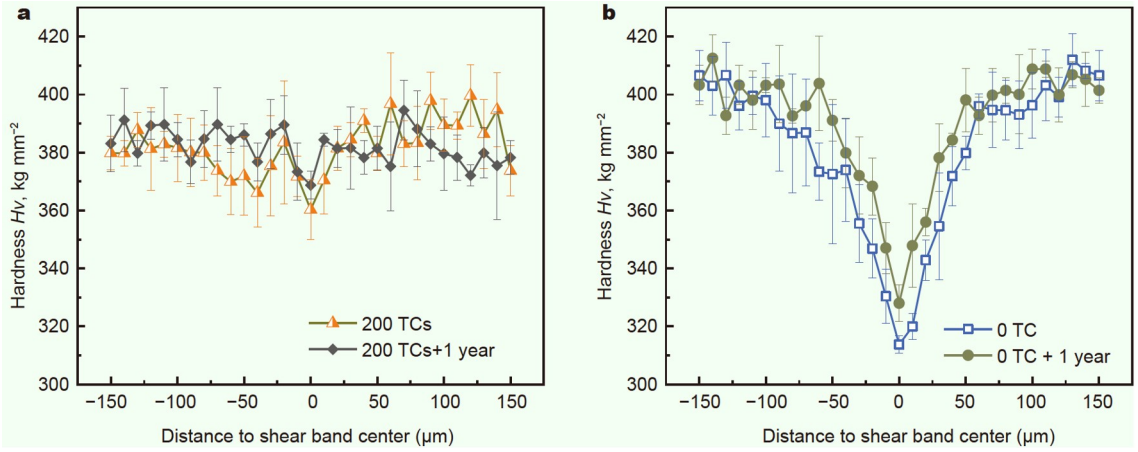

Figure 5 Microhardness (H_V) profile across the SB after aging at the room temperature for one year for the samples undergone (a) 200 TCs; (b) no CTCs.

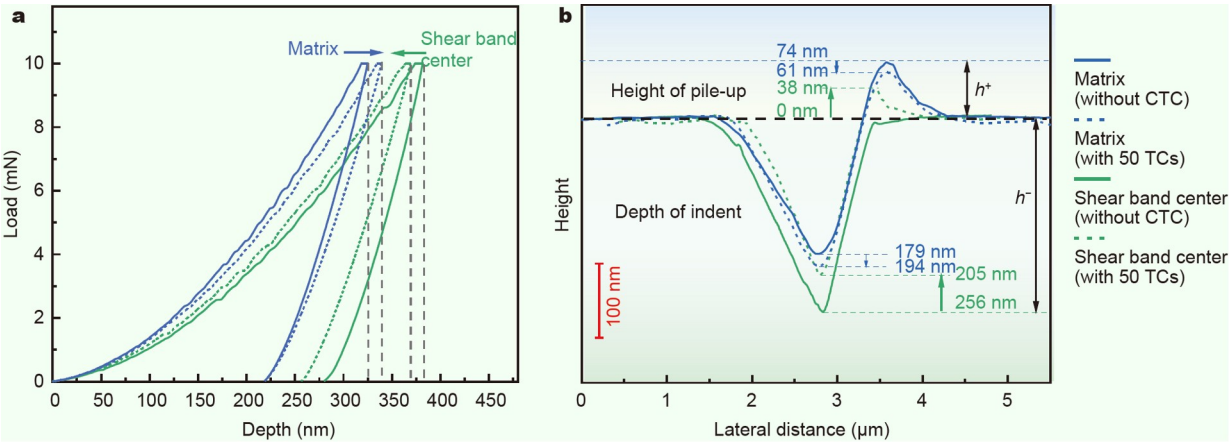

Figure 6 (a) Nanoindentation load (F) *vs.* depth (h) curves of the matrix (blue) and the SB center (green) before (solid) and after (dashed) CTC. (b) AFM profiles of typical indents. The AFM scans were made along a line perpendicular to one edge of the Berkovich indent and crossing its vertex outside the edge.

obtained from the nano-indentation test. The maximum h of the matrix shifts to a higher value when F is 10 mN, while the maximum h of the SB center shifts to a lower value. The F *vs.* h curves of the treated samples (after 50 TCs) collected from the matrix or the SB center also collapse together. The result supports the notion that after CTC, an equilibrium will be reached. Additionally, for the matrix and SB center, respectively, the remaining depth of the indent (h_r) after unloading is 219 and 280 nm. While there is no change in h_r on the matrix after 50 TCs, there is a drop in h_r on the SB center after 50 TCs. This suggests that the equilibrium value of h_r is probably equivalent to that of the matrix.

The AFM analysis characterizes the morphology change of the indents (Fig. 6b). The area around the indent is covered in pile-ups. Prior to the application of CTC, the matrix exhibits a pile-up height (h^+), which refers to the distance between the apex of the pile-up and the sample surface, measuring 74 nm. After 50 TCs, h^+ of the matrix decreases to 61 nm. On the other hand, there are no pile-ups after indenting the SB center before CTC. Following 50 TCs, h^+ increases to 38 nm. When materials are indented, a big h^+ suggests that they are being pushed horizontally, whereas a small (or zero) h^+ suggests that the plastic flow is activated vertically. The depth of the indent center (h^-) shows similar tendencies. The h^- of the SB center is decreased from 256 to 205 nm after 50 TCs, whereas h^- of the matrix is increased from 179 to 194 nm. When the indentation is removed, a small h^- implies a pronounced elastic re-bounce, whereas a high h^- suggests a weak elastic re-bounce. The changes in h^- are highly correlated with changes in h_r. Based on these observations, the SB hardens after CTC, preventing plastic flow beneath the indent [32], whereas the matrix softens after CTC, encouraging plastic flow on the sides of the indent.

DISCUSSION

A free-volume model for CTC

The free-volume model is adapted to CTC under the presumption that CTC causes the MG to deform plastically. It is believed that the structural heterogeneities in the MG frozen from its supercooled liquid at the vitrification point are capable of generating internal shear stress. This internal shear stress is essential in triggering local plastic deformation to the MG even if no external stress is applied to the specimen during CTC. The underlying mechanism is thought to be rooted in the *non-affine* thermal expansion of the MG heterogeneities, leading to internal deformation [16], analogous to the shape change of uranium bars after CTC [33]. Using molecular-dynamics simulation, Lu *et al.* [34] demonstrated that the coefficients of *non-affine* thermal expansion in the 2nd to 3rd nearest atomic shells of $Cu_{50}Zr_{50}$ can be 100% greater or lower than the coefficients of *affine* thermal expansion. Despite the lack of direct evidence, it is reasonable to assume that CTC can indeed induce plastic deformation in MGs.

By modifying the calculation of t, the free-volume model can be adjusted. For plastic deformation, t is the strain (ε) dividing the strain-rate ($\dot{\varepsilon}$). For CTC, MGs would experience plastic deformation for an effective period of t^* during each TC. How to decide t^* remains a question. The plastic deformation is probably caused during the temperature-changing periods of cooling and heating because increasing the holding period at either liquid-nitrogen or room-temperature did not change the extent of rejuvenation [1]. Here, we took 60 s, equivalent to half the total time spent on one TC, as a rough estimation of the temperature-changing period or t^*. Consequently, t equals to the number of cycles (n) times t^*. In order to simplify calculations, $\Delta\dot{x}$ is assumed to be constant throughout each TC. As a result, Equation (9) has been modified as follows:

$$x_n = x_{n-1} + \Delta\dot{x}_n t^*. \tag{10}$$

The determination of x with respect to t is achieved through iterative calculations.

A shear stress τ of 50 MPa (approximately 0.1% of the yield point) is employed in the x calculation. Despite the fact that τ is at such a small magnitude, the computed x exhibits qualitatively similar behavior to the actual results, as shown in Fig. 7. This behavior effectively illustrates how x_0 has an impact on rejuvenation and relaxation. When the value of x_0 is set to 0.08, x increases with increasing n, eventually converging to a steady state value of 0.09 after approximately 110 cycles. In contrast, when the value of x_0 is set to 0.1, x declines with increasing n, stabilizing at 0.09 after about 80 cycles. Notably, an x_0 of 0.08 accords well with the reported x values in as-cast MGs from Refs [35,36], and an x_0 of 0.1 for the SB is feasible given that Maaβ [37] reported that the atomic density of the SB is 2%–8% less

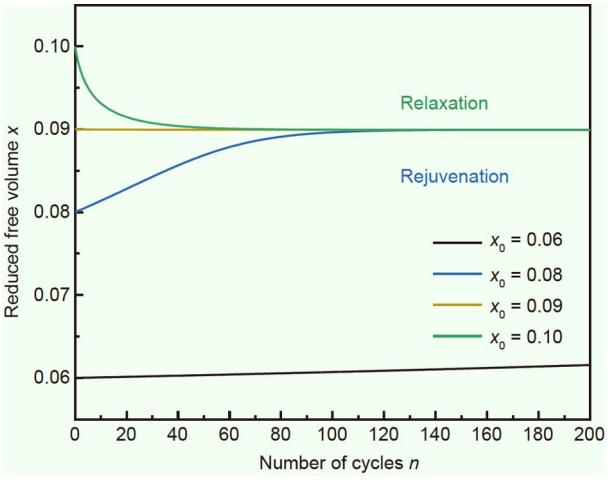

Figure 7 Calculated changes in the reduced free-volume (x) as the number of cycles (n) increases. Depending on the initial x_0 and the equilibrium value, relaxation (decreasing x) or rejuvenation (increasing x) occurs.

than that of the MG matrix. The adapted free-volume model effectively captures our observed phenomena. In cases where the initial x_0 value is small, reflecting the as-cast condition, x increases after undergoing CTC, increasing the stored enthalpy while decreasing sample hardness (Figs 3 and 4b). Conversely, for scenarios where the initial x_0 value is large, as observed in the SB, x drops after undergoing CTC, decreasing the stored enthalpy but increasing sample hardness (Figs 3 and 4b). Finally reaching an equilibrium value in both directions, x produces a constant hardness (Fig. 4b).

The modified free-volume model can also effectively describe a number of other CTC effects. Firstly, CTC appears useless to well-relaxed MGs. A well-relaxed MG starts from a very small x_0, making its $\Delta\dot{x}$ too small to allow for the detection of x-rise. For instance, if an x_0 of 0.06 is used as the input, $\Delta\dot{x}$ of the modeled MG is only 1.1×10^{-7} s^{-1}, and saturation of x requires 2.7×10^5 cycles. Secondly, because $|\Delta\dot{x}|$ increases as x_0 goes up, relaxing from a higher x_0 requires less n than rejuvenation from a lower x_0. This observation can be inferred from Fig. 4b of the hardness measurements because it was discovered that H_V of the MG matrix needs more than 100 cycles to reach equilibrium, whereas the SB only needs 70 cycles for its H_V to reach equilibrium. In addition, it has been demonstrated that 100 cycles are required to rejuvenate a $Pd_{43}Cu_{27}Ni_{10}P_{20}$ MG, but only 60 cycles are need to relax it [4]. Thus, the apparent asymmetry of n for rejuvenation and relaxation results from x_0 of the specimen.

CTC facilitates the relaxation

The TMP theory [22] offers predictions that the CTC effects, i.e., either rejuvenation or relaxation, depend strongly on the initial state of MG. In TMP theory [22], the competition between the temperature and strain rate affects the equilibrium value of ΔH_{rel}. While temperature contributes to the reduction of free volume (reducing ΔH_{rel}), the strain rate contributes to its increase (raising ΔH_{rel}). As a result, if the initial state is above the equilibrium state, relaxation occurs; whereas, if the initial state is below the equilibrium state, rejuvenation occurs. The present work shows that, when CTC is applied to an as-cast MG sample containing an SB, the ΔH_{rel} of the SB (occupying a higher initial state) and the matrix (at a lower initial state) change in the opposite directions and likely merge into an equilibrium value (Fig. 3). Similar trends are also discernible in H_v and various properties related to the indents (Figs 4 and 6). These results confirm the TMP prediction that the initial state, as well as the equilibrium state, matters for the direction of energy change. The starting enthalpy value is a need for rejuvenation; however, Das *et al.* [38] made it clear that CTC cannot rejuvenate well-relaxed MGs. This implies that the TMP theory may be applicable down to a lower enthalpy-limit of the initial state.

It is still a surprise to witness the fact that CTC can cause the SB to relax because SB of the Zr-based MG cannot automatically relax at the temperature range of CTC (from 77 to 353 K). Even if we assume that the annealing temperature is 300 K, it is still only 48% of T_g, which is substantially lower than the conditions applied for conventional thermal annealing [39]. We physically aged compressed specimens, with or without 200 TCs, at 300 K for one year. The results showed negligible H_V change after being annealed (Fig. 5), indicating that the rejuvenation of SB is stable against physical aging at this temperature. Contrary to the "transient" rejuvenation brought on by CTC [40], which would naturally relax under ambient conditions without the necessity for CTC, the high ΔH_{rel} cannot last for longer than one week [4]. As the elevated ΔH_{rel} may be restored to its previous value with fewer TCs than it took to elevate it in the first place, additional TCs added by CTC simply accelerated it [4]. Despite the fact that a pre-request for SB relaxation is an initial state higher than its equilibrium state, it is recognized that CTC can both trigger and facilitate the structural relaxation of SB.

Ketkaew *et al.* [10] studied four as-cast MGs (including the Pd-, Pt-, Zr-, and La-based) and showed that the chemistry of the various alloys had a significant impact on the changes of conditional fracture toughness (K_Q) brought about by CTC. In order to reduce chemical influence and emphasize the structural state, the present work analyzed the SB and MG matrix from the same MG. On the other hand, they also discovered — and this is relevant to this study — that the fictive temperature (T_f) of MGs can affect rejuvenation and relaxation. Their ΔH_{rel} results are consistent with our findings: after 200 TCs on the Pd-based MG, ΔH_{rel} of the high-T_f sample decreased, but that of the low-T_f sample increased. However, K_Q of their Pd-based MG behaved in opposition to the trends we saw, indicating relaxation at a low T_f (implying a smaller x_0) and rejuvenation at a high T_f (implying a higher x_0). In contrast to H_v, it seems that merely providing free volume or x might not be sufficient; instead, additional information from chemical bonding might be needed to capture K_Q responses to CTC. Since it requires more work outside the scope of this study, we limit the use of our model to ΔH_{rel} and H_V, as supported by our experimental results.

CTC releases the residual strain surrounding the SB

It is interesting to note when the TCs are added, the width of the softened regions surrounding the SB center narrows (Fig. 4a). Residual strain leads to softening around the SB, and hence a narrowing SB width denotes the absence of residual strain. At least two things about this observation make it significant. Firstly, it has been suggested that residual strain concentrated at sample surfaces causes CTC-induced rejuvenation. Our findings imply that such residual strain, if present, would be unstable in the presence of CTC. Secondly, stress concentration might cause cracking, which can lead to major issues including sample failure. It is anticipated that the as-cast MGs can get toughened by

CTC if the stress concentrators inside of them are removed, which may already have occurred [9]. It would be useful to conduct more research on the subject of how CTC affects the residual stress of MGs.

According to Hassanpour *et al.* [41], CTC can slightly increase the diffusivities of the bulk MGs that have undergone plastic deformation. Additionally, they discovered that the ΔH_{rel} of the severely deformed samples decreased following CTC (Fig. 3). They therefore imply that while the entire sample is relaxed, the SB center is kinetically rejuvenated. Their observations on structural relaxation are consistent with our data, which reported a decline in ΔH_{rel} (Fig. 3) and a rebound of H_v (Fig. 4a). It is unclear to us if the SB center relaxes after CTC because the sizes of the indent, 10 and 1 μm for the micro- and nano-indentation, respectively, were much bigger than the width of the SB center (approximately 10 nm [42]). It should be noted that even after 100 TCs (Fig. 4a), the H_V measured at the SB center is still lower than that of its surroundings, suggesting that the SB center may not necessarily be relaxed by CTC. The TMP theory, which predicts relaxation when $x_0 > x_{eq}$, a condition that holds for both the SB center and its surrounding areas, appears to be in conflict as a result of this. We suggested, however, that contribution from SB center to the τ that causes x to shift may not be as severe as that of the surrounding region. As a result, the "matrix" in the SB center is probably useless to sustain the flips of too many heterogeneities and hence not creating τ because it requires *non-affine* deformation between the heterogeneities and the "matrix" [4]. Thus, it may be concluded that from a kinetic standpoint, τ dictates whether such changes are conceivable, while from a thermodynamic perspective, x_0 controls the direction of relaxation or rejuvenation.

CONCLUSIONS

The present study examines the effects of initial sample conditions on the directions of energy and property changes of an MG during CTC. By introducing an SB *via* compression, the specimen is specifically created to comprise both rejuvenated and relaxed parts. In this unique setup, the matrix experiences rejuvenation while the SB undergoes relaxation subjected to CTC, as shown by the heat of relaxation, micro-hardness and nano-indentation responses. Notably, after subjecting the specimen to 100 TCs, the enthalpy or property of these two parts merges into a single value. CTC emerges as a catalyst for the relaxation of the SB, distinct from the scenario wherein thermal annealing at the upper limit of the treatment range fails to induce a similar effect. The findings of this study underscore the pivotal role played by the initial conditions of MGs in predicting the propensity for relaxation or rejuvenation as a consequence of CTC.

Received 26 November 2023; accepted 5 January 2024; published online 22 February 2024

1 Ketov SV, Sun YH, Nachum S, *et al.* Rejuvenation of metallic glasses by non-affine thermal strain. Nature, 2015, 524: 200–203
2 Sohrabi S, Ri MC, Jiang HY, *et al.* Prominent role of chemical heterogeneity on cryogenic rejuvenation and thermomechanical properties of La-Al-Ni metallic glass. Intermetallics, 2019, 111: 106497
3 Guo W, Shao Y, Saida J, *et al.* Rejuvenation and plasticization of Zr-based bulk metallic glass with various Ta content upon deep cryogenic cycling. J Alloys Compd, 2019, 795: 314–318
4 Costa MB, Londoño JJ, Blatter A, *et al.* Anelastic-like nature of the rejuvenation of metallic glasses by cryogenic thermal cycling. Acta Mater, 2023, 244: 118551
5 Pan J, Ivanov YP, Zhou WH, *et al.* Strain-hardening and suppression of shear-banding in rejuvenated bulk metallic glass. Nature, 2020, 578: 559–562
6 Guo W, Yamada R, Saida J. Rejuvenation and plasticization of metallic glass by deep cryogenic cycling treatment. Intermetallics, 2018, 93: 141–147
7 Di S, Wang Q, Zhou J, *et al.* Enhancement of plasticity for FeCoBSiNb bulk metallic glass with superhigh strength through cryogenic thermal cycling. Scripta Mater, 2020, 187: 13–18
8 Pan J, Duan F. Rejuvenation behaviors in metallic glasses. Acta Metall Sin, 2021, 57: 439–452
9 Grell D, Dabrock F, Kerscher E. Cyclic cryogenic pretreatments influencing the mechanical properties of a bulk glassy Zr-based alloy. Fatigue Fract Eng Mat Struct, 2018, 41: 1330–1343
10 Ketkaew J, Yamada R, Wang H, *et al.* The effect of thermal cycling on the fracture toughness of metallic glasses. Acta Mater, 2020, 184: 100–108
11 Murali P, Ramamurty U. Embrittlement of a bulk metallic glass due to sub-T_g annealing. Acta Mater, 2005, 53: 1467–1478
12 Ge J, Luo P, Wu Z, *et al.* Correlations of multiscale structural evolution and homogeneous flows in metallic glass ribbons. Mater Res Lett, 2023, 11: 547–555
13 Pan J, Wang YX, Guo Q, *et al.* Extreme rejuvenation and softening in a bulk metallic glass. Nat Commun, 2018, 9: 560
14 Dmowski W, Yokoyama Y, Chuang A, *et al.* Structural rejuvenation in a bulk metallic glass induced by severe plastic deformation. Acta Mater, 2010, 58: 429–438
15 Raghavan R, Boopathy K, Ghisleni R, *et al.* Ion irradiation enhances the mechanical performance of metallic glasses. Scripta Mater, 2010, 62: 462–465
16 Hufnagel TC. Cryogenic rejuvenation. Nat Mater, 2015, 14: 867–868
17 Wang L, Wang Z, Chu W, *et al.* Evolution path of metallic glasses under extensive cryogenic thermal cycling: Rejuvenation or relaxation? Mater Sci Eng-A, 2022, 850: 143551
18 Sohrabi S, Li MX, Bai HY, *et al.* Energy storage oscillation of metallic glass induced by high-intensity elastic stimulation. Appl Phys Lett, 2020, 116: 081901
19 Wang X, Shao Y, Gong P, *et al.* The effect of simulated thermal cycling on thermal and mechanical stability of a Ti-based bulk metallic glass. J Alloys Compd, 2013, 575: 449–454
20 Tang Y, Zhou HF, Wang XD, *et al.* Origin of different thermal cycling effects in $Fe_{80}P_{20}$ and $Ni_{60}Nb_{40}$ metallic glasses. Mater Today Phys, 2021, 17: 100349
21 Kang SJ, Cao QP, Liu J, *et al.* Intermediate structural state for maximizing the rejuvenation effect in metallic glass *via* thermo-cycling treatment. J Alloys Compd, 2019, 795: 493–500
22 Sun Y, Concustell A, Greer AL. Thermomechanical processing of metallic glasses: Extending the range of the glassy state. Nat Rev Mater, 2016, 1: 16039
23 Pan J, Chen Q, Liu L, *et al.* Softening and dilatation in a single shear band. Acta Mater, 2011, 59: 5146–5158
24 Cohen MH, Turnbull D. Molecular transport in liquids and glasses. J Chem Phys, 1959, 31: 1164–1169
25 Heggen M, Spaepen F, Feuerbacher M. Creation and annihilation of free volume during homogeneous flow of a metallic glass. J Appl Phys, 2005, 97: 033506
26 Wang ZT, Pan J, Li Y, *et al.* Densification and strain hardening of a metallic glass under tension at room temperature. Phys Rev Lett, 2013, 111: 135504
27 Duine PA, Sietsma J, van den Beukel A. Defect production and annihilation near equilibrium in amorphous $Pd_{40}Ni_{40}P_{20}$ investigated from viscosity data. Acta Metall Mater, 1992, 40: 743–751
28 Singh S, Ediger MD, de Pablo JJ. Ultrastable glasses from in silico vapour deposition. Nat Mater, 2013, 12: 139–144
29 Jin HJ, Gu XJ, Wen P, *et al.* Pressure effect on the structural relaxation and glass transition in metallic glasses. Acta Mater, 2003, 51: 6219–6231
30 Ma D, Stoica AD, Wang XL. Power-law scaling and fractal nature of

medium-range order in metallic glasses. Nat Mater, 2009, 8: 30–34
31 Liu C, Cai Z, Xia X, *et al.* Shear-band structure and chemistry in a Zr-based metallic glass probed with nano-beam X-ray fluorescence and transmission electron microscopy. Scripta Mater, 2019, 169: 23–27
32 Wu JP, Lin Y, Duan FH, *et al.* Unexpected creep behavior in a rejuvenated metallic glass. J Mater Sci Tech, 2023, 163: 140–149
33 Murty K L, Charit I. An Introduction to Nuclear Materials: Fundamentals and Applications. Berlin: Wiley-VCH, 2013
34 Lu T, Liu SL, Sun YH, *et al.* 1.7 times thermal expansion from glass to liquid. Acta Mater, 2023, 242: 118450
35 Xu Y, Fang J, Gleiter H, *et al.* Quantitative determination of free volume in $Pd_{40}Ni_{40}P_{20}$ bulk metallic glass. Scripta Mater, 2010, 62: 674–677
36 Wang JG, Zhao DQ, Pan MX, *et al.* Correlation between onset of yielding and free volume in metallic glasses. Scripta Mater, 2010, 62: 477–480
37 Maaß R. Beyond serrated flow in bulk metallic glasses: What comes next? Metall Mater Trans A, 2020, 51: 5597–5605
38 Das A, Dufresne EM, Maaß R. Structural dynamics and rejuvenation during cryogenic cycling in a Zr-based metallic glass. Acta Mater, 2020, 196: 723–732
39 Zheng Q, Zhang Y, Montazerian M, *et al.* Understanding glass through differential scanning calorimetry. Chem Rev, 2019, 119: 7848–7939
40 Derlet PM, Maaß R. Micro-plasticity in a fragile model binary glass. Acta Mater, 2021, 209: 116771
41 Hassanpour A, Vaidya M, Divinski SV, *et al.* Impact of cryogenic cycling on tracer diffusion in plastically deformed $Pd_{40}Ni_{40}P_{20}$ bulk metallic glass. Acta Mater, 2021, 209: 116785
42 Greer AL, Cheng YQ, Ma E. Shear bands in metallic glasses. Mater Sci Eng-R-Rep, 2013, 74: 71–132

Acknowledgements Pan J and Sun Y thank Prof. A.L. Greer from the University of Cambridge for useful discussion. This work was supported by the National Natural Science Foundation of China (52022100, 52192604, 51971097, 51971239 and 92263103). Pan J also acknowledges the financial support from the Key R&D Program of Hubei (2022BAA023) and Basic Research Support Program of Huazhong University of Science and Technology (5003110121), and Sun Y acknowledges the support from the Young Elite Scientists Sponsorship Program by China Association for Science and Technology. The authors are grateful to the Analytical and Testing Center, Huazhong University of Science and Technology for technical assistance.

Author contributions Liu L and Pan J designed and supervised the project. Wei Y prepared and characterized the samples. Sun Y contributed to the theoretical analyses and free volume calculation. Li N and Zhang C performed the data analyses. Wang W provided significant guidance on the study. Wei Y, Pan J and Sun Y wrote the paper. All authors contributed to the general discussion.

Conflict of interest The authors declare that they have no conflict of interest.

Yufeng Wei is a PhD candidate supervised by Prof. Jie Pan at the School of Materials Science and Engineering, Huazhong University of Science and Technology (HUST). His research interest mainly focuses on the rejuvenation behaviors in metallic glasses.

Jie Pan is now a full professor at HUST. He received his PhD degree from HUST in 2011. His research interests include the designing and mechanical behavior of bulk metallic glasses, high-entropy alloys, and gradient nanostructured metallic materials.

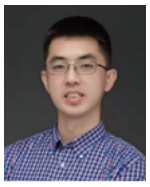

Yonghao Sun is currently an associate professor at the Institute of Physics, Chinese Academy of Sciences. He received his PhD degree from the University of Cambridge in 2016. His research interest focuses on thermo-mechanical processing of metallic glasses.

Lin Liu is currently a Huazhong-distinguished professor at HUST, he is also a chief professor at the State Key Lab for Materials Processing and Die & Mold Technology. His research interests mainly focus on metallic glasses, amorphous alloy coatings, metal nano-porous materials, and additive manufacturing.

低温热循环加速非晶合金剪切带在室温的结构弛豫

魏玉锋[1], 潘杰[1,2*], 孙永昊[3,4*], 李宁[1], 张诚[1], 汪卫华[3,4], 柳林[1*]

摘要 低温热循环是实现非晶合金结构回春的一种简单有效方法，但某些非晶合金在低温热循环处理后发生弛豫而不是回春. 本研究通过在非晶合金中引入剪切带，在同一块样品上获得了不同区域初始能量不同的非晶合金，系统地研究了不同初始状态对低温热循环处理效果的影响. 研究结果发现，在经过低温热循环处理后，同一试样中的剪切带发生结构弛豫，而基体发生结构回春. 类似的双向变化趋势还可以从显微硬度、纳米压痕曲线以及压痕形状的变化上得到验证. 经历了100次低温热循环处理后，剪切带和基体的焓和硬度均收敛到一个平衡值. 低温热循环能够加速剪切带的结构弛豫，实现了在低温热循环的上限温度上做长时间退火所达不到的状态. 文中还采用自由体积模型对实验结果进行分析，阐明了非晶合金的初始状态影响其结构演化方向的机理. 本研究为低温热循环处理非晶合金提供了新见解，阐明非晶合金初始状态在其焓变方向上的关键作用.

